Elastic modulus versus cell packing density in MDCK epithelial monolayers

Steven J. Chisolm [a] , Emily Guo [b], Vignesh Subramaniam [a], Kyle D. Schulze [b], Thomas E. Angelini [a,c,d,*]

[a] Department of Mechanical and Aerospace Engineering, University of Florida, Gainesville, FL 32605, United States
[b] Department of Mechanical Engineering, Auburn University, Auburn, AL 36849, United States
[c] Department of Materials Science and Engineering, University of Florida, Gainesville, FL 32605, United States
[d] J. Crayton Pruitt Family Department of Biomedical Engineering, University of Florida, Gainesville, FL 32605, United States

A B S T R A C T

The elastic moduli of tissues are connected to their states of health and function. The epithelial monolayer is a simple, minimal, tissue model that is often used to gain understanding of mechanical behavior at the cellular or multi-cellular scale. Here we investigate how the elastic modulus of Madin Darby Canine Kidney (MDCK) cells depends on their packing density. Rather than measuring elasticity at the sub-cellular scale with local probes, we characterize the monolayer at the multi-cellular scale, as one would a thin slab of elastic material. We use a micro-indentation system to apply gentle forces to the apical side of MDCK monolayers, applying a normal force to approximately 100 cells in each experiment. In low-density confluent monolayers, we find that the elastic modulus decreases with increasing cell density. At high densities, the modulus appears to plateau. This finding will help guide our understanding of known collective behaviors in epithelial monolayers and other tissues where variations in cell packing density are correlated with cell motion.

1. Introduction

The elasticity of living cells is intimately coupled to their function across different states of tissue health, development, and disease. For example, in the lung and the breast, cancerous tissue often exhibits a significantly lower elastic modulus than healthy functional tissue (Cross et al. 2020). During body axis elongation in zebrafish embryos, developing tissue exhibits spatially varying material properties, where elasticity at one end preserves supracellular structure while dominantly fluid-like behavior at the other end enables cell rearrangements and flow during extension and growth (Mongera et al. 2018). Gradients in cell size, number density, and cell elasticity have been found to correlate to the aggressiveness of tumor invasion into the surrounding microenvironment (Han et al. 2020). To guide our interpretation of these complex phenomena, simple *in vitro* cellular models are often employed for highly controlled experimentation and the testing of theories. For example, much of our current understanding of the relationship between cell packing density and patterns of motion came from studies of monolayers as model tissues (Angelini et al. 2010, Angelini et al. 2011, Bi et al. 2015, Bi et al. 2011, Chisolm et al. 2024, Nnetu et al. 2012, Tambe et al. 2011, Trepat et al. 2009). While a great deal of focus has been given to motion and mechanical forces in monolayers, much less is known about the relationship between packing density and elastic

modulus. The elastic modulus of individual cells in monolayers have been measured using methods such as magnetic twisting cytometry (MTC), in which a rotating magnetic field applies torsion to ferromagnetic beads attached to the cytoskeleton (Barry et al. 2015, Overby et al. 2014, Trepat et al. 2006). Similarly, magnetic tweezers (MT) have been used to determine cytoskeletal material properties by driving magnetic beads contained inside the cells within monolayers (Huang et al. 2005). By using atomic force microscopy (AFM), it was found that the elastic modulus of human umbilical vein endothelial cells (HUVECs) increased with increasing spread area, mediated by cell–cell cohesion (Stroka and Aranda-Espinoza 2011). While microscopic techniques like MTC, MT, and AFM have enabled measurements of elasticity of isolated cells and cells in monolayers, it is not clear how these measurements at the sub-cellular scale are related to the elasticity of monolayers or tissues when tested as macro-scale materials. Few investigations of the material properties of monolayers at multi-cellular scales have been performed (Schulze et al. 2017), and a systematic investigation of monolayer elasticity at different cell packing densities remains to be carried out. Making the connection between monolayer elasticity at multi-cellular scales and cell packing density would represent a valuable step toward understanding the hierarchical relationships that determine tissue mechanics in health and disease.

In this manuscript we investigate the relationship between the elastic

---

modulus and cell number density in a model epithelial monolayer. We perform indentation measurements on confluent islands of Madin Darby Canine Kidney cells, collecting force-indentation curves on layers prepared at different seeding densities, indenting approximately 100 cells in each measurement. We find the force-indentation profiles exhibit a strong dependence on cell density, and we employ a simple contact mechanics model to determine their elastic moduli. We find that the elasticity of MDCK monolayers decreases with increasing cell number density within the lower range of densities, plateauing in the higher range. Given the well-established connection between collective motion in monolayers and cell density, our findings indicate that cell density fluctuations may be accompanied by spatiotemporal patterns of varying elasticity that mediate cell–cell coupling and the patterns in collective motion that emerge.

2. Results

2.1. Micro-indentation tests on cell monolayers

To create epithelial monolayers for indentation tests, we seed cells at various number densities onto collagen-coated glass-bottomed culture dishes. We vary the number density by depositing 2 μL droplets of liquid growth media containing MDCK cells dispersed at different concentrations. Once the cells have adhered, we gently add 2 mL of culture media to the dishes and incubate overnight. Within the cell density range explored here, there are no gaps between cells; the islands are confluent. To enable cell density to be determined, we dye the confluent islands with 5-chloromethylfluorescein diacetate (CMFDA). Indentation experiments are performed on an inverted microscope equipped with a heated stage that maintains the culture dishes at 37 °C. The indenting probe-tip is a 1 mm diameter hemisphere made from borosilicate glass coated in F-127 Pluronic which prevents adhesion to the cells. The probe tip is manually positioned approximately 2 μm above the apical surface of the monolayer and translated downward at a rate of 1 μm/s, indenting the monolayers by approximately 3 μm at the tip's apex. The indentation force and indentation depth are recorded at a rate of 5000 Hz while fluorescence images are simultaneously recorded (see Methods for instrument details). We use these images to assess the condition of the monolayers before, during, and after indentation, ensuring the process causes no damage. Additionally, we only indent each region of cells one time (Fig. 1).

Here we chose to focus on short timescale responses to contact forces for several reasons. First, there is a large body of literature reporting oscillatory shear measurements on *ex vivo* tissue samples which are performed at frequencies near 1 Hz (van Oosten et al. 2019). Thus, the indentations occurring over timescales of seconds allow comparison to previous work. At slightly longer timescales, we previously showed that indentation forces applied for many minutes drives fluid out of the cells under contact, which enabled measurements of cell–cell permeability (Schulze et al. 2017). It will be interesting to study permeability as a

function of cell density in the future, but here we focus on monolayer elasticity. At even longer timescales, over the course of hours, cells spontaneously fluctuate in size, shape, and cytoskeletal organization, so indentation measurements over comparable scales are not expected to capture passive material properties but instead will reflect actively generated forces.

To determine whether the elastic modulus of monolayers depends on cell density, we analyze each force–displacement (*F-d*) dataset and we perform image analysis to measure the cell number density of the corresponding monolayer. Briefly, cell density is measured using a machine-learning based image segmentation software, Cellpose 2.0 (Stringer et al. 2021), employing the pre-trained Cyto2 model. The number of identified cells is divided by the area of the field of view to determine the cell number density. For indentation measurements, the fields of view corresponded to the indented regions. For monolayer thickness measurements, described later, all cells in each image were counted. Automatic cell counting was validated by a comparison to hand counting, finding roughly 3 % error. Representative data collected on monolayers having different number densities demonstrate that the indentation force, *F*, rises more rapidly with increasing indentation depth, *d*, than for monolayers at lower densities (Fig. 2a). Fluorescence images of monolayers prepared at different densities can be seen in Fig. S1.

To determine an elastic modulus from each measured *F-d* dataset, we restrict our analysis to the smallest range of indentation depths over which a sufficiently large dynamic range of measured forces occurs across all samples. Working in the thin-slab limit, we estimate the estimate the average normal strain in the monolayer to be given by $\langle \gamma \rangle = \langle d \rangle / h$, where h is the monolayer thickness and the angle brackets indicate an average over the contacting surface area. It can be shown that that $\langle d \rangle = d_{max}/2$ for a spherical indenter where d_{max} is the indentation depth at the apex of the indenter. Thus, by limiting d_{max} to 2.4 μm, the average strain in the monolayer at the high end of the indent is 0.2 for a representative monolayer having a thickness of $h = 6$ μm. Our analysis below indicates that the monolayers remain in the linear elastic regime during indentation measurements when employing this strategy.

2.2. Correlation analysis of noisy force-indentation curves

We find that that the noise amplitude in *F-d* measurements is approximately ± 10 μN, which could potentially reduce our confidence in determining the elastic modulus of many monolayers, especially those in the higher density range. Thus, we do not directly fit a contact mechanics model to any of the measured *F-d* curves. Instead, to systematically analyze the *F-d* curves collected for the full range of prepared monolayer densities, even those with high noise-to-signal ratios, we employ a method previously developed for determining elastic moduli from extremely noisy data (O'Bryan et al. 2019, O'Bryan et al. 2024). The method minimizes the contribution of noise to the analysis by comparing the autocorrelation functions of *F* and *d*, rather than directly
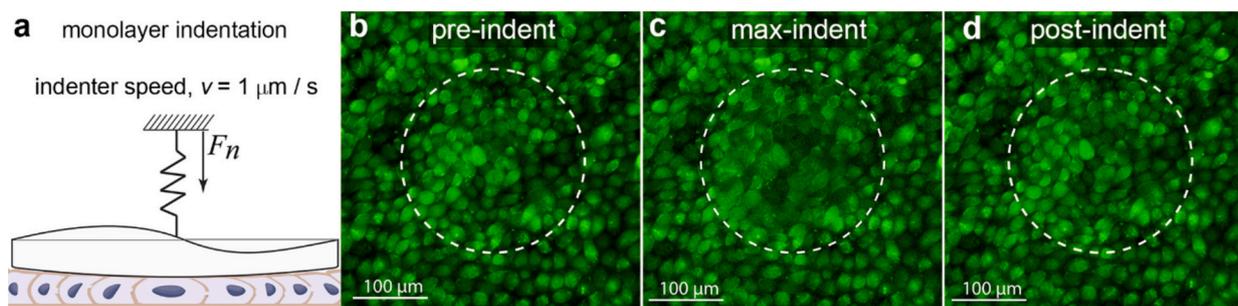
Fig. 1. Monolayer micro-indentation experiments. (a) A micro-indenter is mounted above an inverted microscope. The hemispherical indentation probe moves at a rate of 1 μm/s as it indents the MDCK monolayer. The instrument records the normal force and the indentation depth throughout the experiment. (b) Images of the monolayer collected prior to indentation, (c) at the maximum indentation depth, (d) and a short time after indentation.
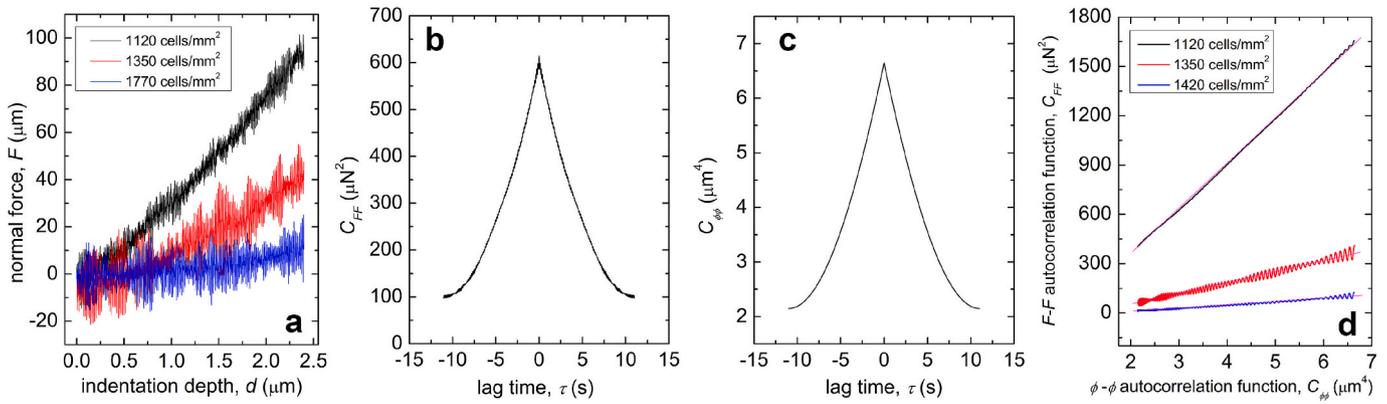
Fig. 2. Indentation and autocorrelation analysis. (a) Force-displacement curves of indented monolayers exhibit high levels of noise. (b) Plots of the force auto-correlation function, C_{FF}, demonstrate how statistical averaging reduces the contribution of random noise in our analysis method. (c) The autocorrelation function of $\phi = d^2$, $C_{\phi\phi}$, visibly resembles C_{FF} and exhibits even less noise. (d) Plots of C_{FF} vs $C_{\phi\phi}$ for monolayers having different densities exhibit linear trends. The indentation modulus of each monolayer is determined linear regression analysis of these plots (magenta lines overlaying data are linear fits).

fitting F-d curves. The analysis method accounts for the contribution of noise, modeling data with a general expression for the measured force, given by

$$F(t) = K\phi(t) + n(t) + F_0$$

where $\phi(t) = d^p(t)$, K contains the elastic modulus and other constants, $n(t)$ is random noise with zero mean, and F_0 is an unknown constant offset in the force data. The power p and the parameters that constitute K depend on the contact mechanics model that is employed to analyze the F-d data. Here, we employ the Winkler contact model in which $F \sim d^2$, so $p = 2$. The Winkler model is appropriate to use in contexts where the test material is a very thin slab, having a thickness much less than the contact width; previous results on MDCK monolayers support this choice (Schulze et al. 2017). We will discuss the details of K later. By computing the autocorrelation function of both sides of the $F(t)$ equation, the random noise term is eliminated, as are many cross-terms, yielding a simple relationship between the F and ϕ autocorrelation functions, given by

$$C_{FF}(\tau) = K^2 C_{\phi\phi}(\tau) + \beta$$

where C_{FF} is the F autocorrelation function, $C_{\phi\phi}$ is the ϕ autocorrelation function, and β is a combination of constants. Thus, K can be determined from a linear regression of C_{FF} versus $C_{\phi\phi}$.

A representative plot of C_{FF} shows the effect of computing the autocorrelation function; a small, sharp drop between $\tau = 0$ and the first time-shift reflects the noise amplitude, while the rest of the curve is dominated by the shape of the F profile. We also note that small and regularly spaced oscillations are visible in $C_{FF}(\tau)$, which likely arise from weak vibrations of the micro-indentation cantilever (Fig. 2b). In contrast to C_{FF}, we see no noticeable drop in $C_{\phi\phi}$ around $\tau = 0$, and we see no visible oscillations (Fig. 2c). Thus, measurements of d exhibit much less noise and are much less susceptible to mechanical vibrations than measurements of F. Eliminating τ and parametrically plotting C_{FF} versus $C_{\phi\phi}$, we find a clear linear relationship between the two parameters. The oscillations observed in $C_{FF}(\tau)$ can be seen superimposed on the C_{FF} versus $C_{\phi\phi}$ curves, but do not appear to diminish the linearity of the trends; the slopes of these curves equal K^2, which we determine using linear regression (Fig. 2d). With this method, we are able to determine the monolayer's elastic modulus without directly fitting the F-d curves.

2.3. Relationship between monolayer elastic modulus and cell density

The clear linearity between C_{FF} and $C_{\phi\phi}$ provides confidence that the Winkler model captures the elasticity of monolayers over short time-scales; the duration from the first point of contact to the final

datapoint we include in our analysis is just 2.4 s, which is much shorter than that time-scales of active contraction and stiffening of cells in response to applied forces (Fernández et al. 2006). The F-d relationship given by the Winkler model is

$$F = \pi E^* \frac{R}{h} d^2$$

so the relationship between E^* and the best fit values of K^2 is given by

$$E^* = \frac{hK}{\pi R}$$

where R is the radius of the hemispherical indenting probe and h is the monolayer thickness. We previously measured the thickness of MDCK monolayers at individual densities in the range of 1400 cells/mm², finding the typical monolayer thickness to be approximately 6 μm. To determine whether E^* varies with cell density, we performed thickness measurements on a series of monolayers seeded at different cell concentrations. Monolayers were prepared in the same way as for indentation tests, described above. Using a 60x oil-immersion objective, we collected laser-scanning confocal z-stacks of fluorescently labeled monolayers (Fig. 3a).

The basal location of each monolayer was determined by manually choosing the first plane in which the monolayer came into focus; using a z-step size of 0.1 μm enables this procedure to be performed with a high degree of certainty, since the basal side of the monolayer is flat. To estimate the location of the apical side of the monolayer, we averaged the 3D fluorescence intensity stack along the X and Y axes, creating an intensity profile along the Z-axis, $I(z)$ (Fig. 3b). Normalizing by the maximum intensity of $I(z)$, we estimated the top location of the monolayer by identifying where the normalized intensity drops from its maximum value of 1 to a value of 0.5. We performed a sensitivity analysis of this method, choosing thresholds of 0.35 and 0.75 instead of 0.5, finding that the pattern in thickness versus density does change significantly, apart from re-scaling all measured heights by a single factor of 1.4 and 0.67, respectively. The choice of 0.5 results in heights within the range of previous investigations of monolayer thickness, which also showed that the method described here produces the same result as averaging over many local measurements of height (Zehnder et al. 2015a). In that work it was found that cell volumes changed dramatically without major height fluctuations. On an individual cell-by-cell basis, it was noted that with increasing cell density some cells slightly increased in height and others slightly decreased in height. However, the question of whether the taller cells, on average, are found in higher density regions was not systematically investigated. Notably, it was found that cell volumes dynamically fluctuate by about $\pm$ 20 %
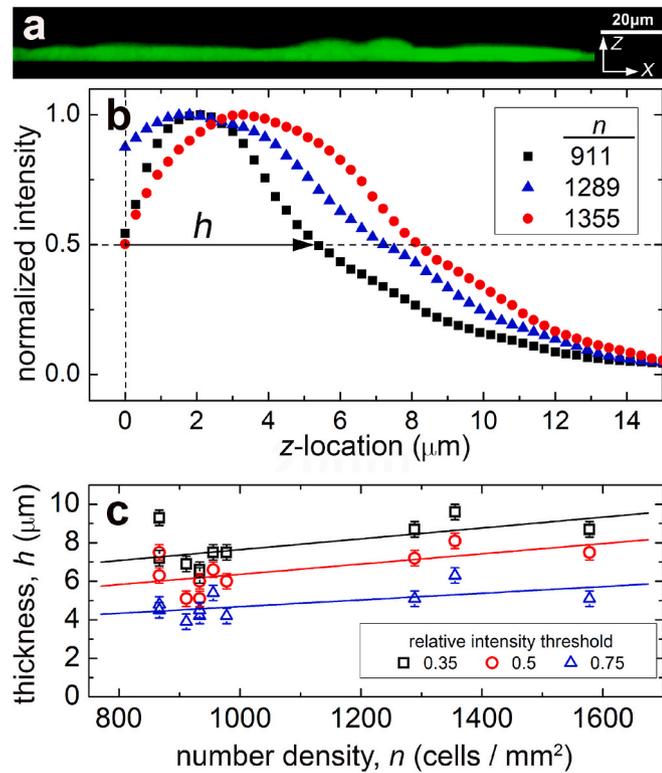
Fig. 3. Monolayer thickness measurement. (a) X-Z projections of confocal z-stacks show the relatively flat and sporadically bumpy apical surfaces of dyed monolayers, as well as their extremely flat basal surfaces adhered to glass ($n = 1355$ cells / mm^2 for this sample). (b) The 3D confocal fluorescence intensity profiles are averaged in the X-Y plane to create intensity profiles along the z-axes of monolayers. The location of the half-maximum intensity value is used to determine the monolayer thickness. (c) Monolayer thickness exhibits a weak dependence on cell number density. Here we show thickness profiles for three different intensity thresholds and simultaneous linear fits to all datapoints (reduced $\chi^2 = 0.97$). The uncertainty intervals denote $\pm$ depth of field of the microscope objective. These data represent measurements on ten different monolayer islands.

about their means. Here, by approximating cell volume as h/n and comparing the lowest densities and the highest densities, we find that the average cell volume changes by about 25 % across the density range explored.

We find that the monolayer thickness varies weakly with cell density. By fitting a line through these datapoints, we create a mapping between cell density and monolayer thickness, which we use to determine E^* from our F-d measurements (Fig. 3c). We tested the sensitivity of the fitted line to the unevenness of the distribution of datapoints by excluding the extrema in the cluster of data in the low-density range and re-fitting. Comparing the originally fitted line with lines fit to subsets of data in which either two or four extrema were excluded, we found approximately 2 % difference in both cases. Plotting E^* versus n, we find that the indentation modulus decreases within increasing cell density in the lower density range, dropping from approximately 30 kPa to about 7 kPa before plateauing at high densities (Fig. 4).

The plateau in elastic modulus at high cell densities led us to consider whether cells undergo a qualitative change in their aspect ratio. From our measurements of monolayer height and cell density, we find that, within the range explored here, the monolayers do not exhibit any major phenotypic transitions in the 3D shapes of the cells they comprise. Estimates of a height-to-diameter aspect ratio fall within a range of 0.16 to 0.28, always reflecting a plate-like shape. At no densities do we see groups of cells near a 1:1 cuboidal aspect ratio or near a columnar aspect ratio that would be greater than 1. While the aspect ratio is only
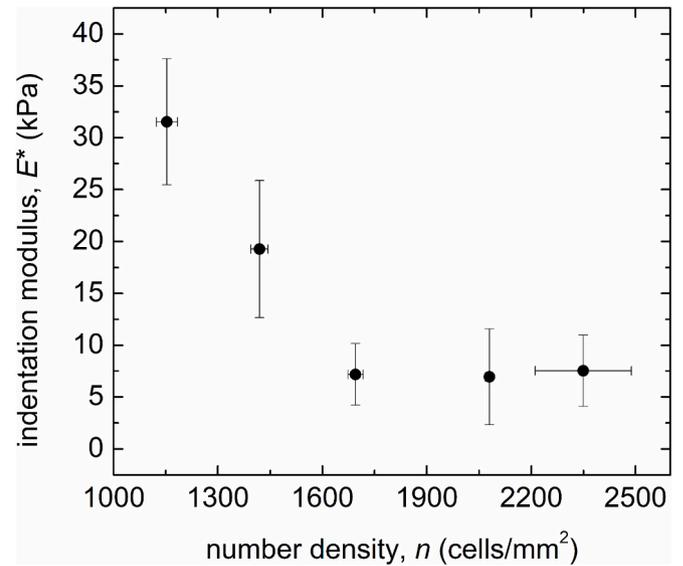
Fig. 4. Plot of indentation modulus, E^*, vs measured number density, n. We find a trend of decreasing modulus with increasing density until it reaches a plateau of approximately 7 kPa at higher densities (datapoints and intervals correspond to the mean $\pm$ standard error averaged over $N = 2$–9 replicate experiments).

modestly changed, it is likely that changes in cytoskeletal organization accompany increases in cell density, where the ratio of cortical to basal actin may vary, particularly in the circumferential belt of actin that mediates the force balance between cells.

3. Discussion

In this manuscript we have investigated how the elastic modulus of epithelial monolayers depends on cell packing density. By employing an analysis method that was developed for use with extremely noisy data, we were able to determine the elastic moduli of very soft monolayers that indented to strains of 20 % in response to only 10 μN of applied normal load. The results of this analysis method confirmed the choice of the Winkler contact model for interpreting F-d curves, as expected from basic geometric considerations and from previous measurements on monolayers prepared at a single density (Schulze et al. 2017). Part of this analysis required measuring the monolayer thickness as a function of density, which we found only to exhibit a weak increase with increasing cell number density.

The most significant finding of this study is that the monolayer's elastic modulus decreases with increasing cell number density in the low-density regime and appears to plateau at the highest densities. Previous work has shown that the elastic modulus of single isolated cells increases with their spread area (Chaudhuri et al. 2015, Nisenholz et al. 2014, Stroka and Aranda-Espinoza 2011), as does the modulus of single cells in monolayers. Thus, our work shows that the monolayer at multi-cellular scales, when tested like an inanimate material slab, exhibits a trend consistent with the previous work characterizing single cells, whether isolated or in monolayer. Each of our indentation experiments simultaneously measure anywhere between a few cells and a few hundred cells throughout an individual F-d curve. For example, when using a hemispherical indentation probe having a radius of 1 mm, the contact width at the maximum indentation depth, $d = 2.4$ μm, is approximately $2a = 140$ μm, where $a = \sqrt{2Rd}$. It is noteworthy that this contact width is comparable to the characteristic length-scales of giant cell density fluctuations, previously studied in MDCK layers (Zehnder et al. 2015a, Zehnder et al. 2015b, Zehnder et al. 2016). The work presented here indicates that such giant density fluctuations are likely accompanied by spatially heterogeneous distributions of elastic modulus. In contrast to

many passive materials that generally stiffen in non-linear regimes of compression, these results suggest that cells may dynamically soften as they concentrate in the monolayer, tipping toward mechanical instability and leading to giant density fluctuations that are characteristic of active matter (Narayan et al. 2007).

The potential connection between dynamic fluctuations in cell density and elasticity suggests additional connections to patterns of motion and cell shape within monolayers. For example, as cell density rises in MDCK monolayers, their motion becomes arrested and they exhibit several hallmarks of the glass transition (Angelini et al. 2011). Reevaluating glassiness in dense monolayers while accounting for a density-dependent elastic modulus could reveal new differences between tissue-cell dynamics and collective behaviors in classical molecular or colloidal glasses. Similarly, transitions between fluid-like and solid states with changes in cell shape are predicted by multiple models of monolayers (Bi et al. 2015, Bi et al. 2016). Such a transition has been observed experimentally in lung epithelia where a threshold in cell shape was crossed while unjamming occurred (Park et al. 2015). Cell shape is typically thought to be determined by a balance between cortical tension and the level of cell–cell cohesion. Recent work showed the systematic change in cell shape with changes in cell density and cohesion (Chisolm et al. 2024). In that work, it can be seen that the monolayers with unmodified levels of cohesiveness, like those studied here, cross a threshold where migration speed switches from increasing to decreasing as packing density increases beyond about 1600 cells/mm^2. At this density, a dimensionless shape factor crosses a threshold of 3.81 that demarcates a rigidity transition (Chisolm et al. 2024). This is the same density where we see the plateau in elastic modulus appear (Fig. 4). Thus, the softening of monolayers with increased cell density found here is most likely accompanied by changes in cell shape and thus may contribute to transitions in collective patterns of motion within monolayers and transitions between fluid-like and jammed states. Since the states of collective motion in monolayers are so strongly tied to cell shape through the level of cell–cell cohesion, moving forward we plan to investigate how monolayer elasticity at the multi-cellular scale is determined by the combination of cell–cell cohesion and cell density.

4. Materials and methods

4.1. Cell culture and island seeding

Madin Darby canine kidney (MDCK) epithelial cells are cultured in Dulbecco's modified Eagle's medium (DMEM) supplemented with 10 % fetal bovine serum (FBS) and 1 % penicillin–streptomycin, maintained at 37 °C in a 5 % CO2 atmosphere. The cells are grown approximately 70 % confluence in six-well plates then harvested using standard trypsinization protocols. The dispersed cells are pelleted with gentle centrifugation and resuspended in 175 μL of fresh culture medium. To create monolayer islands, several 2 μL droplets of the cell suspension are deposited in a grid-like pattern near the center of a glass-bottomed petri dish coated with molecular collagen-1 and incubated for 30 min to allow cell attachment. 2 mL of fresh culture media is added to the dish, which is then incubated for an additional 12–24 h before commencing time-lapse imaging. To enable observation of the cells during indentation, the monolayers are treated with a dye solution containing 5-chloromethyl-fluorescein diacetate (CMFDA) and dimethyl sulfoxide (DMSO) in serum-free and antibiotic-free DMEM for 30 min. After dye treatment, the cells are washed with and returned to culture media.

To prepare dishes coated with molecular collagen, 35 mm culture dishes having microscope coverslips as their base (Cellvis, product #: D35-20–1.5H) are exposed to 200 Watts UV light for 5 min. Molecular collagen at a concentration of 6 mg/mL (Nutragen Type I Collagen Solution, Advanced Biomatrix 5010) is diluted with milli-Q water to a concentration of 0.04 mg/mL. 175 μL of the diluted collagen solution is pipetted onto the coverglass region of the dish and left at room temperature for 30 min. The collagen solution is aspirated and the dish is washed with PBS buffer then air dried in a bio safety cabinet before cell islands are deposited.

4.2. Micro-Indentation instrument

To perform indentations on MDCK monolayers we designed a micro-indentation system that mounts to the condenser arm of an inverted microscope, in place of the condenser lens turret. This design facilitates the alignment of the indentation probe with the optical axis. The indentation system is made from a capacitance sensor, a piezo-controlled z-stage, and a rigid indentation probe mounted onto a calibrated cantilevered flexure. The probe indents the surface of the monolayer as the stage downward, bending the cantilever. Cantilever deflection creates a voltage change measured by the capacitance sensor. We measure the voltage from the indentation onto the monolayers using a voltage input module (National Instruments NI 9220) and compact DAQ (National Instruments cDAQ-9171). This DAQ collects the voltage measurements at 5000 Hz. The linear positioner (Physik Instrumente P-628.1CD) used to move the probe has an 800 μm travel range with 1 nm resolution. Custom-written MATLAB code translates the piezo-stage while collecting position and voltage data. The voltage is converted to a force using the measured cantilever stiffness. Indentation depth is determined by computing the difference between piezo stage position and cantilever deflection.

We selected regions of the islands for indentation where we saw no evidence of cell division or floating cells. Since the M phase of the cell cycle lasts about one hour and the typical division time of cells in culture is about 24 h, we would expect about four out of every 100 cells to be actively dividing. Dividing cells typically look more rounded-up than interphase cells. This relatively small population allows us to avoid regions where cells appear to be rounded up or detached from the surface.

CRediT authorship contribution statement

Steven J. Chisolm: Methodology. **Emily Guo:** Writing – review & editing, Methodology, Investigation, Formal analysis. **Vignesh Subramaniam:** Methodology, Investigation. **Kyle D. Schulze:** Methodology. **Thomas E. Angelini:** Writing – review & editing, Supervision, Project administration, Methodology, Investigation, Funding acquisition, Formal analysis, Data curation, Conceptualization.

Declaration of competing interest

The authors declare that they have no known competing financial interests or personal relationships that could have appeared to influence the work reported in this paper.

Acknowledgement

Appendix A. Supplementary data

Supplementary data to this article can be found online at https://doi.org/10.1016/j.jbiomech.2025.112648.

References

Angelini, T.E., Hannezo, E., Trepat, X., Fredberg, J.J., Weitz, D.A., 2010. Cell Migration Driven by Cooperative Substrate Deformation Patterns. Physical Review Letters 104, 168104.

Angelini, T.E., Hannezo, E., Trepat, X., Marquez, M., Fredberg, J.J., Weitz, D.A., 2011. Glass-like dynamics of collective cell migration. Proceedings of the National Academy of Sciences 108, 4714–4719.

Barry, A.K., Wang, N., Leckband, D.E., 2015. Local VE-cadherin mechanotransduction triggers long-ranged remodeling of endothelial monolayers. Journal of Cell Science 128, 1341–1351.

Bi, D., Lopez, J., Schwarz, J.M., Manning, M.L., 2015. A density-independent rigidity transition in biological tissues. Nature Physics 11, 1074–1079.

Bi, D., Yang, X., Marchetti, M.C., Manning, M.L., 2016. Motility-driven glass and jamming transitions in biological tissues. Physical Review X 6, 021011.

Bi, D., Zhang, J., Chakraborty, B., Behringer, R.P., 2011. Jamming by shear. Nature 480, 355–358.

Chaudhuri, O., Gu, L., Darnell, M., Klumpers, D., Bencherif, S.A., Weaver, J.C., Huebsch, N., Mooney, D.J., 2015. Substrate stress relaxation regulates cell spreading. Nature Communications 6, 6365.

Chisolm, S.J., Guo, E., Subramaniam, V., Schulze, K.D., Angelini, T.E., 2024. Transitions between cooperative and crowding-dominated collective motion in non-jammed MDCK monolayers. Cells & Development.

Cross, S.E., Jin, Y.-S., Rao, J., Gimzewski, J.K., 2020. Nanomechanical analysis of cells from cancer patients. Nano-enabled medical applications, Jenny Stanford Publishing, pp. 547–566.

Fernández, P., Pullarkat, P.A., Ott, A., 2006. A master relation defines the nonlinear viscoelasticity of single fibroblasts. Biophysical Journal 90, 3796–3805.

Han, Y.L., Pegoraro, A.F., Li, H., Li, K., Yuan, Y., Xu, G., Gu, Z., Sun, J., Hao, Y., Gupta, S. K., 2020. Cell swelling, softening and invasion in a three-dimensional breast cancer model. Nature Physics 16, 101–108.

Huang, H., Sylvan, J., Jonas, M., Barresi, R., So, P.T., Campbell, K.P., Lee, R.T., 2005. Cell stiffness and receptors: evidence for cytoskeletal subnetworks. American Journal of Physiology-Cell Physiology 288, C72–C80.

Mongera, A., Rowghanian, P., Gustafson, H.J., Shelton, E., Kealhofer, D.A., Carn, E.K., Serwane, F., Lucio, A.A., Giammona, J., Campàs, O., 2018. A fluid-to-solid jamming transition underlies vertebrate body axis elongation. Nature 561, 401–405.

Narayan, V., Ramaswamy, S., Menon, N., 2007. Long-Lived Giant Number Fluctuations in a Swarming Granular Nematic. Science 317.

Nisenholz, N., Rajendran, K., Dang, Q., Chen, H., Kemkemer, R., Krishnan, R., Zemel, A., 2014. Active mechanics and dynamics of cell spreading on elastic substrates. Soft Matter 10, 7234–7246.

Nnetu, K.D., Knorr, M., Käs, J., Zink, M., 2012. The impact of jamming on boundaries of collectively moving weak-interacting cells. New Journal of Physics 14, 115012.

O'Bryan, C.S., Schulze, K.D., Angelini, T.E., 2019. Low force, high noise: Isolating indentation forces through autocorrelation analysis. Biotribology 20, 100110.

O'Bryan, C.S., Ni, Y., Taylor, C.R., Angelini, T.E., Schulze, K.D., 2024. Collagen Networks under Indentation and Compression Behave Like Cellular Solids. Langmuir 40, 4228–4235.

Overby, D.R., Zhou, E.H., Vargas-Pinto, R., Pedrigi, R.M., Fuchshofer, R., Braakman, S.T., Gupta, R., Perkumas, K.M., Sherwood, J.M., Vahabikashi, A., 2014. Altered mechanobiology of Schlemm's canal endothelial cells in glaucoma. Proceedings of the National Academy of Sciences 111, 13876–13881.

Park, J.-A., Kim, J.H., Bi, D., Mitchel, J.A., Qazvini, N.T., Tantisira, K., Park, C.Y., McGill, M., Kim, S.-H., Gweon, B., 2015. Unjamming and cell shape in the asthmatic airway epithelium. Nature Materials 14, 1040–1048.

Schulze, K.D., Zehnder, S.M., Urueña, J.M., Bhattacharjee, T., Sawyer, W.G., Angelini, T. E., 2017. Elastic modulus and hydraulic permeability of MDCK monolayers. Journal of Biomechanics 53, 210–213.

Stringer, C., Wang, T., Michaelos, M., Pachitariu, M., 2021. Cellpose: a generalist algorithm for cellular segmentation. Nature Methods 18, 100–106.

Stroka, K.M., Aranda-Espinoza, H., 2011. Effects of morphology vs. cell–cell interactions on endothelial cell stiffness. Cellular and Molecular Bioengineering 4, 9–27.

Tambe, D.T., Corey Hardin, C., Angelini, T.E., Rajendran, K., Park, C.Y., Serra-Picamal, X., Zhou, E.H., Zaman, M.H., Butler, J.P., Weitz, D.A., 2011. Collective cell guidance by cooperative intercellular forces. Nature Materials 10, 469–475.

Trepat, X., Puig, F., Gavara, N., Fredberg, J.J., Farre, R., Navajas, D., 2006. Effect of stretch on structural integrity and micromechanics of human alveolar epithelial cell monolayers exposed to thrombin. American Journal of Physiology-Lung Cellular and Molecular Physiology 290, L1104–L1110.

Trepat, X., Wasserman, M.R., Angelini, T.E., Millet, E., Weitz, D.A., Butler, J.P., Fredberg, J.J., 2009. Physical forces during collective cell migration. Nature Physics 5, 426–430.

van Oosten ASG, et al. 2019. Emergence of tissue-like mechanics from fibrous networks confined by close-packed cells. Nature 2019 573:7772 573:96-101.

Zehnder, S.M., Suaris, M., Bellaire Madisonclaire, M., Angelini, T.E., 2015a. Cell Volume Fluctuations in MDCK Monolayers. Biophysical Journal 108, 247–250.

Zehnder, S.M., Wiatt, M.K., Urueña, J.M., Dunn, A.C., Sawyer, W.G., Angelini, T.E., 2015b. Multicellular density fluctuations in epithelial monolayers. Physical Review E 92, 032729.

Zehnder, S.M., Zegers, F.M., Angelini, T.E., 2016. A Langevin model of physical forces in cell volume fluctuations. Journal of Biomechanics 49, 1286–1289.